ANL/IPNS/PP--82562

RECEIVED
NOV 12 1996
OSTI

Heat Generation and Neutron Beam Characteristics in A High Power Pulsed Spallation Neutron Source

Dong W. Jerng* and John M. Carpenter
Intense Pulsed Neutron Source
Argonne National Laboratory
Argonne, Illinois 60439, U.S. A.
Tel) 708-252-5519
Fax) 708-252-4163

The submitted manuscript has been authored by a contractor of the U. S. Government under contract No. W-31-109-ENG-38. Accordingly, the U. S. Government retains a nonexclusive, royalty-free license to publish or reproduce the published form of this contribution, or allow others to do so, for U. S. Government purposes.

* currently at : Nuclear Division
Korea Electric Power Corp. Research Center
108-11 Munji-Dong
Yusong-Ku, Taejon
Korea, 350-380
Tel) 82-42-865-5632
Fax) 82-42-865-5214

DISTRIBUTION OF THIS DOCUMENT IS UNLIMITED

HH

MASTER

DISCLAIMER

Portions of this document may be illegible in electronic image products. Images are produced from the best available original document.

DISCLAIMER

This report was prepared as an account of work sponsored by an agency of the United States Government. Neither the United States Government nor any agency thereof, nor any of their employees, makes any warranty, express or implied, or assumes any legal liability or responsibility for the accuracy, completeness, or usefulness of any information, apparatus, product, or process disclosed, or represents that its use would not infringe privately owned rights. Reference herein to any specific commercial product, process, or service by trade name, trademark, manufacturer, or otherwise does not necessarily constitute or imply its endorsement, recommendation, or favoring by the United States Government or any agency thereof. The views and opinions of authors expressed herein do not necessarily state or reflect those of the United States Government or any agency thereof.

Abstract

In the course of conceptual design of a high power pulsed spallation source, a Monte Carlo model was developed for heat generation and neutronics studies. In this paper, we present two sets of results. The first set of calculations was performed with a simple target model to investigate general characteristics of power distribution and neutron production with various proton energies ranging from 0.8 to 12 GeV. The second set was performed with a realistic target model including major components of the target system to provide basic parameters for engineering design of a high power pulsed spallation source. Calculated results generally confirm that higher proton energy provides an advantage in target cooling system requirements and yet somewhat lower neutron beam intensity as a counter effect. The heat generation in the systems surrounding the target was investigated in detail and found to have important variation with position and according to proton beam energy. Calculations of the neutron currents from the moderators showed that the neutron beam intensity from moderators in the front region of the target decreased for higher proton energy while that from moderators in the back region of the target remained almost unchanged.

I. Introduction

Pulsed spallation neutron sources produce neutrons from heavy metals such as tungsten and uranium on which high energy protons from an accelerator impinge in a pulsed mode. In recent years, pulsed spallation neutron sources have attracted increasing attention because of their applications in materials research using neutron scattering, for example, ceramic superconductors, amorphous materials, strains in composite materials and for applications such as radiation therapy, radiation effects on materials, and radioisotope production. In these and many more applications, spallation neutron sources are both comparable and complementary to nuclear reactor sources A recent Workshop examined these uses in considerable detail [1].

The neutron source in the present study consists of a two-part split target with a vacuum region in-between called a "flux trap" and six moderators. The proton beam has 1 MW time-averaged power with protons of 2.2 GeV energy. The facility is intended to deliver slow neutron fluxes five times higher than any currently operating facility in the world. The power distributions and the neutron beam characteristics in such a high power pulsed neutron source are the main results of this paper. Although 2.2 GeV is the proposed energy of protons for the high power spallation source currently under consideration, a calculation with 9 GeV protons was also performed to investigate the effects of such relatively high proton energies on the heat load and neutron generation. Also, a series of calculations using an idealized target system was performed to provide insight to the relationship between impinging proton energy and the distribution of power and neutrons. This calculation also served as a benchmark for the validation of the code system and physical models used in the Monte Carlo method.

We used the LAHET code system as the computing tool for these Monte Carlo calculations. The LAHET system has been developed in Los Alamos National Laboratory (LANL) and mainly consists of an LANL version of the high energy transport code (HETC) and the general Monte Carlo code for neutron and photon transport (MCNP) with several associated codes [2]. LAHET calculates the high energy particle cascade, including neutrons, at energies above 20 MeV. MCNP transports photons and neutrons below 20 MeV, with the neutron and photon source files generated by LAHET.

A validation of the LAHET code system and physical model was performed for two parameters which were of most interest for our objectives: the energy deposition in the target and the neutron production rate. For the validation, the target was modeled as 20 disks of 5 cm thickness and 10 cm diameter with a 2 mm gap between disks for water coolant. The target was housed in a stainless steel structure imbedded in the beryllium reflector. The proton beam was assumed of a Gaussian distribution truncated at 4 cm in radius with the full-width-at-half-maximum (FWHM) radius of 2 cm. The target was 1 m long, sufficient to encompass the stopping length of energetic protons. Tantalum was assumed for the target material. The results from the present study were compared with the available data in the

literature[3,4]. Fig. 1 shows the calculated ratio of energy deposited in the target to the energy carried in by the proton beam. Considering the small difference in mass and nuclear composition between lead and tantalum, it is concluded that Fig. 1 confirms the validity of the LAHET code system and physical models used in the calculation. Fig. 2 shows the neutron production rate in the tantalum target compared with that in the lead target. It is seen that the neutron production rate is a little higher with tantalum than with lead. We conclude that the computer code and physical models set up for this study are sound enough for the next stage calculation. We realize that the high energy transport code with its treatment of particle interactions at high energies has not been validated for energies above about 3.5 GeV. Nevertheless, we have performed calculations for proton energies up to 12 GeV on the strength of the observation that no new thresholds are crossed between 3.5 and 12 GeV, so that the results should be at least qualitatively correct.

II. Heat Deposition and Neutron Production with Various Proton Energies

To investigate the effects of proton energy on the power deposition and neutron production in the target, we calculated power density and neutron current distributions with several proton energies up to 12 GeV. The target model and proton beam conditions used in this series of calculations was the same as used for the code validation except that the target length was extended to 2 m for the calculations with 6 and 12 GeV protons. The results are summarized in Table 1. Figs. 3 and 4 show the spatial distributions of power density and neutron currents. Both functions show characteristic features of the high energy nucleon cascade, namely a nearly energy-independent falloff with distance in the target, which comes about because at these energies the dominant interactions are nuclear collisions rather than electronic energy loss, while the cross sections are nearly independent of energy. Both show a buildup from the front of the target to a maximum at a distance not very deep into the target, which increases with the proton

energy and comes about because the particle cascade tends toward an equilibrium dominated by the energy-independent collision rate of the incident proton beam.

It should be noted that for Table 1 and Figs. 3 and 4, the power densities are the values averaged over disks of 5 cm radius and 5 cm thickness and the neutron currents represent the outgoing neutrons evaluated at the surface of the target housing at 6.2 cm radius. From Table 1, higher proton energy yields higher neutron production per proton but the neutron production rate normalized to 1 MW proton beam power is found to be peaked at 1.5 GeV and slowly decreases as the proton energy increases. It is seen in Figs. 3 and 4 that the location of the maximum power density occurs in the first disk and that of the maximum neutron current occurs at the second disk.

The total power deposited in the target is found to be almost constant, i.e., between 60 and 70 % of beam power, as long as the target dimension is sufficiently large to exhaust the particle cascade. The fluctuations of the power density and neutron current near the end of the target shown in Figs. 3 and 4 are due to the statistical uncertainty of the Monte Carlo calculation, since few particles remain at the deeper location in the target.

One of the important design considerations for the spallation source target is to obtain a maximum neutron current as high as possible while the maximum power density is maintained as low as attainable. Fig. 5 shows the variation of the maximum neutron current and of the maximum power density as functions of the proton energy. The data shown in Fig. 5 are normalized values to the results for 0.8 GeV protons. The maximum neutron current and maximum power density show the same trend, i.e., both decrease as the proton energy increases. The normalized ratio of the maximum neutron current to maximum power density increases as proton energy increases from 0.8 to 1.5 GeV protons but does not change significantly for proton energies higher than 1.5 GeV.

III. High Power Target Station Model

The target station including targets, moderators, and neutron beam lines was modeled with a reflector and shield surrounding these components.

Table 2 lists the geometrical and material features of key components modeled for Monte Carlo simulation. An isometric view of the target and moderators is shown in Fig. 6 and the labels for six moderators are also indicated in Fig. 6. Fig. 7 shows a plan view of the target station from the top for the illustration of neutron beam lines. The moderators and neutron beam lines are covered by boron decouplers to cut off thermal neutrons scattered into the beam lines from the reflector. There are three neutron beams from each moderator totaling 18 beam lines in the target station. The beam lines are separated by an angle of 15°. Fig. 8 shows the arrangements of the reflector, shield and removable assemblies for remote handling systems.

For all calculations in the subsequent sections, the proton beam centered on the axis of the target was assumed to be truncated at 5 cm radius with a Gaussian distribution of 2.5 cm FWHM radius. The calculations described in subsequent sections are normalized results based on a time average 1 MW proton beam power.

IV. Power Distribution in the Target Station

The power distribution in the components of the target station is summarized in Table 3. With 2.2 GeV protons, about 90 % of the beam power is deposited in the target station and the 10 % is thought either to be absorbed in the form of binding energy resulting from the change of isotope compositions during the cascade process or to escape through neutron and photon leakage. For instance, the number of neutrons escaping from the outer boundaries of the system in the model is about 9.7 neutrons/proton. Assuming 8 MeV for the neutron binding energy, this leak constitutes about 35 kW/MW-beam. Thus, the overall energy balance is thought to be satisfied in the calculation. The overall energy balance was also confirmed in the case of 9 GeV protons. In this case, about 95 % of the beam power was deposited in the target station and 5 % is thought to be absorbed as binding energy or to escape the system. For both proton energies, the total power deposited in the target was found to be the same, i.e., about 55 % of the proton beam power is deposited in the target material.

For the heat deposition in the moderators, there is a considerable difference between 2.2 and 9.0 GeV protons. Since the volume of the upstream moderators is half that of the flux trap or second target moderators, the power densities of the moderators are approximately THE same for 2.2 GeV protons regardless of their locations, i.e., about 1.5 W/cm^3. For 9.0 GeV protons, however, the power density of the first target moderators is about 53 % of the second target moderators. The decrease of the power density in the first target moderators is consistent with the decrease of the neutron beam intensity as will be seen in Fig. 16.

The spatial distributions of the heat deposition within the moderators have been investigated because the power density, around 1.5 W/cm^3, is so high, especially for cryogenic moderators, as to invite special treatment, say by inclusion of premoderators. Fig. 9 shows the spatial heat deposition at the first upstream moderator in the vertical and horizontal directions relative to the target axis. The heat deposition decreases rapidly in the vertical direction as the distance from the target increases (Fig. 9a) while it is almost uniform in the horizontal direction (Fig. 9b). It is noticed in Fig. 9a that about 30 % of the heat deposited in the moderator appears in the region labeled as pre-moderator which is only 17 % of the total moderator volume; more than 50 % of the heat is deposited in the 4 cm thick layer adjacent to the target. Thus, it may be possible to reduce the heat load by more than 50 % with the insertion of a pre-moderator region of water 4 cm thick between the target and moderator.

Table 4 shows a comparison of the key results from 2.2 GeV and 9.0 GeV protons. The neutron yield per proton is much higher for 9.0 GeV protons. However, the neutron production rate per MW-beam is higher for 2.2 GeV protons. This is partly because the target dimensions are not adequate to utilize all the energy of 9.0 GeV protons and partly because energy is lost from the hadronic cascade in the form of π^0's, which quickly decay to energetic photons. (This "electromagnetic drain" on the cascade is known to limit the rate of hadronic process as a function of proton inergy, to vary roughly as $E^{0.8}$ for energies above a few GeV.) The maximum power density is lower for 9.0 GeV protons because of the longer stopping length for higher energy protons. Higher energy protons penetrate deeper in the target and

deposit more energy in the back of the target than lower energy protons. Fig. 10 shows a comparison of the axial power distribution in the target for 2.2 and 9.0 GeV protons. It is noticed in Fig. 10 that the peak power occurs in the first disk for 2.2 GeV protons but it occurs in the second disk for 9.0 protons. This seems to augur favorably for higher proton energies in that for fixed beam power, proton beam windows should be less subject to radiation damage. Also, it is observed that the power in the first target is higher for 2.2 GeV protons but the power in the second target is higher for 9.0 GeV protons.

We have further analyzed the power distribution in the reflector and shield as illustrated in Figs. 11 and 12. The front and back segments of the reflector are approximately the same in size while the middle segment is much smaller. Also, the shield is segmented in the same manner as the reflector. Hence, it is noticed in Figs. 11 and 12 that the heat deposited in the back of both reflectors and shield is much greater than in the front. The anisotropic power distribution in the reflector and shield is more significant with 9.0 GeV protons, for instance, the power in the back half of the shield is seven times larger than the power in the front half of the shield. This spatial distribution of heat load in the surroundings of the target calls special attention not only to the cooling system design but also to radiation protection considerations because higher heat load indicates higher radiation dose as well. For the heat load in the back of the shield, the heat deposited by high energy particles (i.e., heat load calculated by LAHET) is 1.5 times higher than that deposited by low energy neutrons (i.e., heat load calculated by MCNP) for 2.2 GeV protons. The ratio of the two heat depositions, i.e., LAHET calculated heat to MCNP calculated heat is 2.1 for 9.0 GeV protons. Thus, the heat deposited by escaping protons and cascade particles other than low energy neutrons becomes more dominant for higher proton energies. The statistical uncertainty of the calculation shown in Table 3 is less than 3 % for the target power and maximum 10 % for the individual moderator powers.

V. Neutron Beam Characteristics

Figure 13 compares, the neutron current spectra outgoing from the surface of the six moderators for the case of 2.2 GeV protons. It is seen in Fig. 13 that the shapes of neutron spectra are almost the same for all six moderators and that the first moderators result in the highest neutron current in all energy bins. Fig. 14 shows the neutron spectra at the end of the center beam lines from the first target, flux-trap, and second target moderators. We show no details of the spectra of thermal neutrons; the totals appear in the lowest energy bin. These details depend on the specific design of the moderators, that is, moderator material, temperature, and poisoning, however, it turns out that the epithermal spectrum is relatively insensitive to these specifics, which are determined by the requirements of instruments that view the moderators but are relatively difficult to model. Measurements or calculations of the low energy spectra performed in simplified geometries, which extend into the epithermal regime, can be attached to the higher-energy spectra to provide reasonably accurate representations of the spectra in the full range of interest when normalized at epithermal energy (say, at 1. eV.)

At the end of beam lines, the neutron beam from the flux-trap moderator is slightly higher than those from the other two moderators especially for the thermal energy region. The change of the neutron beam spectrum along the beam line from the moderator surface to the end of the beam lines, about 85 ~ 90 cm away from the moderator surfaces (the boundary of the model) is shown in Fig. 15. The neutron beam intensity becomes smaller as it approaches the end of beam line over the entire range of neutron energy as expected. However, the ratio of thermal to fast neutrons decreases most significantly in the decoupling region, that is, from the moderator to the end of the decoupler (see Fig. 7). The decoupler cuts off thermal neutrons coming into the beam line from the reflector while it is transparent to fast neutrons.

The total number of neutrons produced in the target is 49 neutrons per proton with 2.2 GeV protons.

A comparison of neutron beam characteristics between 2.2 and 9.0 GeV protons is shown in Fig. 16. A noticeable effect of higher proton energy is that a larger fraction of neutrons appear in the back region of the target. As seen in Fig. 16, the neutron spectrum from the first target moderator decreases over the entire range of neutron energy for the change of proton energy from 2.0 to 9.0 GeV while that from the second target moderator remains little changed. The shapes of neutron spectra from all moderators are almost identical regardless of impinging proton energies. This is thought to indicate that the volume of moderators used in the calculation is adequate to attain an equilibrium spectrum regardless of the source neutron spectrum generated in the target. The statistical errors of the Monte Carlo calculations are less than 7 % for the neutron beams at moderators for all energy bins.

VI. Conclusions

We have investigated the effects of proton energy on the heat load and neutron yield in the target. The results have shown that higher proton energy offers an advantage in target cooling because the maximum power density is lower. However, the neutron production rate and maximum neutron current at a given proton beam power were observed to be reduced if proton energy is higher than 1.5 GeV. The ratio of the maximum neutron current to maximum power density increased as the proton energy increased from 0.8 to 1.5 GeV but did not change significantly for the proton energy greater than 1.5 GeV.

The total power deposited in the target was found to be insensitive to proton energy. The ratio of the target heat load to proton beam power was approximately 0.6 to 0.7 with targets in which the dimension was sufficient to stop the proton beam and exhaust the cascade process. This same conclusion as to the target heat load follows from calculations on the realistic target model in the current study.

For the power distribution in the surrounding systems, i.e., in the reflector and shield, we found a large variation of heat load with respect to position. The heat load was much higher in the back of the target system

than in the front and this non-uniform distribution of heat load was more noticeable for higher proton energy. Thus, the cooling of the surroundings needs to take account of the spatial variation of heat load.

The characteristics of neutron beam spectra from moderators in the realistic target model did not change significantly with different proton energies. The proton energy was found to affect the magnitude of neutron beam intensity depending on the location of a moderator, i.e., higher proton energy resulted in lower neutron beam intensity from the moderators installed at the front of the target. Thus, the location of moderators around the target may be differently optimized depending on the proton beam energy.

Acknowledgment

The financial support of the Argonne National Laboratory on this work is greatly appreciated and the authors are grateful to Dr. R. E. Prael in Los Alamos National Laboratory for providing the LAHET code system and many technical suggestions.

REFERENCES

1. G. Aeppli and B. S. Brown, "Technology and Science at a High-Power Spallation Source," Proceedings of a Workshop held at Argonne National Laboratory May 13-16, 1993, U. S. Government Printing Office 1994-547-499 (February, 1994).

2. Richard E. Prael and Henry Lichtenstein, "User Guide to LCS: the LAHET Code System", LA-UR-89-3014, Los Alamos National Laboratory, Sept. 1989.

3. T. W. Armstrong et al, "Theoretical Target Physics Studies for the SNQ Spallation Neutron Source", Jül-Spez-120, KfK Karlsruhe, Germany, July 1981.

4. N. Watanabe et al, "Report of the Moderator Working Group", International Workshop on the Technology of Targets and Moderators for Medium to High Power Spallation Neutron Sources, Paul Scherrer Institute, Switzerland, Feb. 1992.

Table 1. Calculation summary (based on 1-MW Beam except neutron yield)

Proton energy (GeV)	Neutron yield per proton	Neutron production rate ($x10^{17}$n/sec)	Maximum neutron current [a] ($x10^{14}$ n/cm^2 /sec)	Maximum power density [b] (kW/cm^3)	Total power deposition in the target (MW)
0.8	16.3	1.28	2.0	0.604	0.692
1.5	33.6	1.41	1.90	0.477	0.627
2.2	48.8	1.39	1.80	0.439	0.619
3.0	64.4	1.34	1.65	0.415	0.626
6.0	115.6	1.20	1.39	0.371	0.654
12.0	194.8	1.01	1.25	0.307	0.656

[a] neutron current at the cylindrical surface (radius: 6.2 cm) of the target housing

[b] power density averaged over a disk (radius: 5 cm and thickness: 5 cm) of the target

Table 2. Geometrical and material features of the key target station components

Component	Geometry and Dimension	Material
Target	split target: four elliptic disks [a] in the first target nine elliptic disks [a] in the second target	tantalum
Housing	rectangle with rounded side surfaces: first target housing: 18 cm wide, 12 cm high, 12 cm long second target housing: 18 cm wide, 12 cm high, 40 cm long, (spring at the back)	0.5 cm thick stainless steel
Flux Trap	18 cm void section between the housings	vacuum
Coolant	coolant channel gap between target disks: 0.2 cm	water
Moderator	first target moderators: 5 cm x10 cm x 10 cm flux trap moderators: 5 cm x10 cm x 20 cm second target moderators: 10 cm x 10 cm x 10 cm	water
Boron Decoupler	2 cm thick layer surrounding moderators and neutron beam lines	aluminum, 3.3 w/o natural boron [b]
Reflector	cylinder: r = 54 cm, h = 100 cm	beryllium
Shield	annulus: r_i = 54 cm, r_o = 100 cm, h = 100 cm	iron

[a] minor radius = 5.5 cm, major radius = 7.5 cm, thickness = 2.5 cm (first target), 3.5 cm (second target)

[b] boron density for a decoupling energy of 1.0 eV and 1/e reduction of neutron flux perpendicularly crossing the decoupler.

Table 3. Heat deposition in the components of the target station for 1 MW proton beam

Component	Heat Deposition (kW) by 2.2 GeV protons	Heat Deposition (kW) by 9. GeV protons
Target	550.8 (total)	553.6 (total)
first target	306.5	251.0
second target	244.3	302.6
Coolant	21.0	14.5
Housing	34.2	40.0
Moderator [a] Total	7.6 (total)	6.4 (total)
first top moderator	0.775	0.413
first bottom moderator	0.773	0.417
flux trap moderator - right	1.516	1.30
flux trap moderator - left	1.498	1.27
second top moderator	1.582	1.54
second bottom moderator	1.477	1.50
Boron Decoupler	26.7	20.1
Reflector	126.6	120.4
Shield	128.0	187.0
Removable Assembly	7.0	6.6
Target Station Total	901.9	948.6

[a] see Fig. 6 for the location of moderators around the target.

Table 4. A comparison of key results between 2.2 and 9.0 GeV protons

Proton energy (GeV)	Neutron yield per proton	Neutron production rate per MW-beam	Maximum power density [a] (kW/cm^3) per MW-beam
2.2	49.3	1.40×10^{17} n/sec	1.650 in the first disk
9.0	151.5	1.05×10^{17} n/sec	1.216 in the second disk

[a] the power density in the central region with r = 1 cm

Figure Captions

Fig. 1 A validation of IPNS Upgrade calculation model - heat deposition in targets

(Source for other than IPNS upgrade calculation : Reference 3)

Fig. 2 A validation of IPNS Upgrade calculation model - neutron generation rate

(Source for European Spallation Source Study : Reference 4)

Fig. 3 Power density along the target depth for various proton energies

Fig. 4 Neutron current along the target for various proton energies

Fig. 5 Ratio of the maximum neutron current to maximum power density for various proton energies

Fig. 6 Configurations of targets and moderators

Fig. 7 Arrangement of neutron beam lines

Fig. 8 Schematic of the systems surrounding the targets

Fig. 9 (a) Power distribution of the moderator in the vertical direction

Fig. 9 (b) Power distribution of the moderator in the horizontal direction

Fig. 10 Axial power distribution along the target

Fig. 11 Power distribution in the reflector

Fig. 12 Power distribution in the shield

Fig. 13 Neutron beam spectra at the moderator surfaces

Fig. 14 Neutron beam spectra at the end of beam lines

Fig. 15 Change of neutron beam spectrum along the beam line

Fig. 16 Effect of proton energy on neutron beam spectra

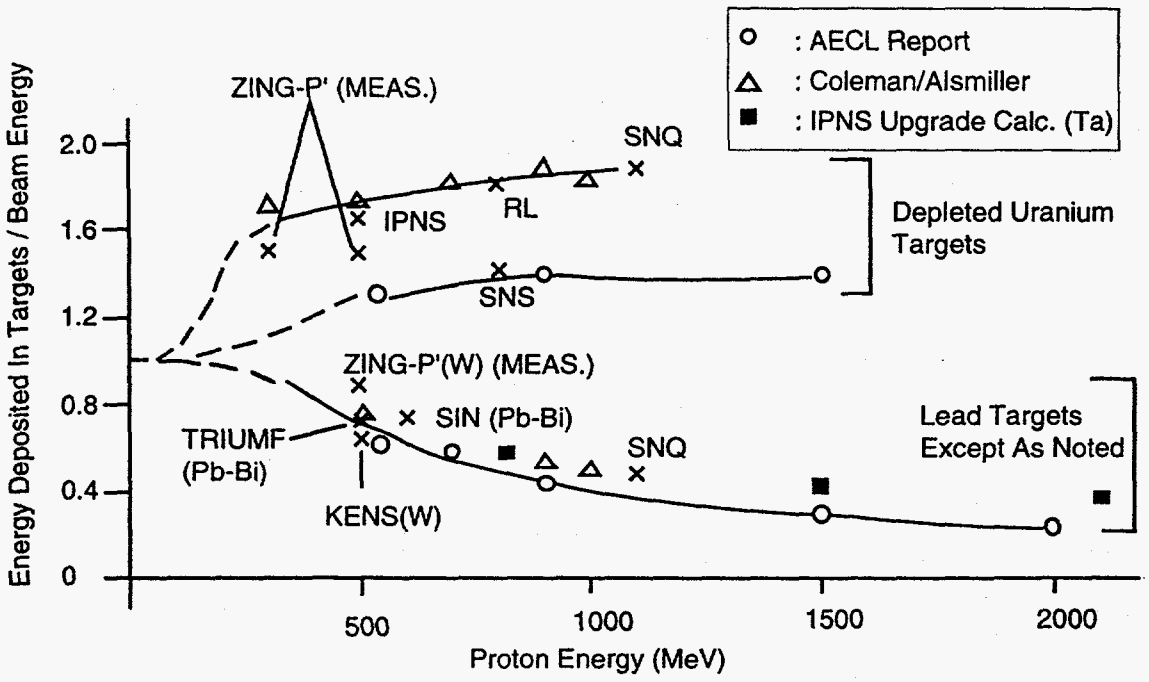

Fig. 1 A validation of IPNS Upgrade calculation model - heat deposition in targets
(Source for other than IPNS upgrade calculation : Reference 3)

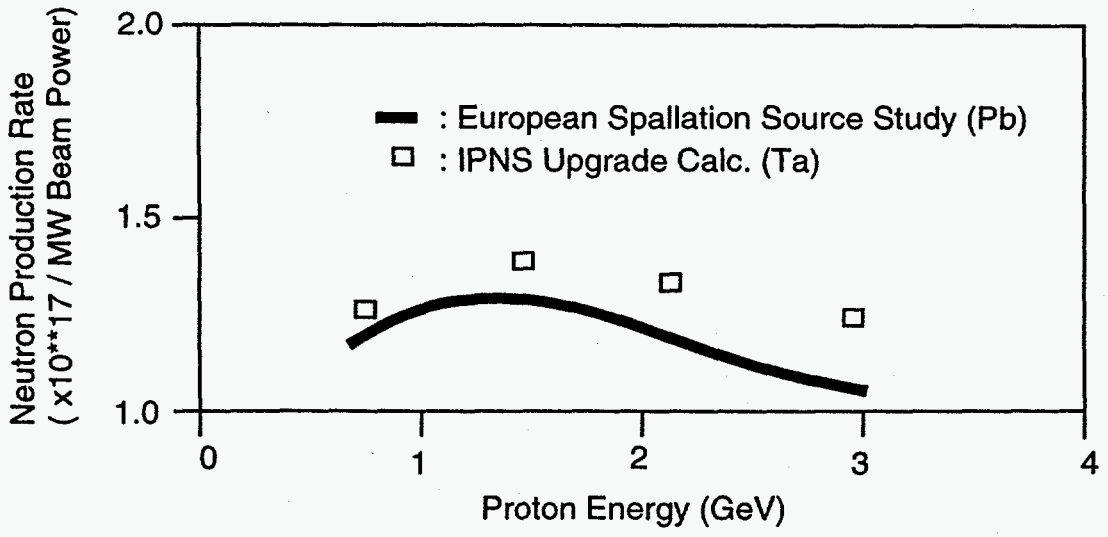

Fig. 2 A validation of IPNS Upgrade calculation model -
- neutron generation rate
(Source for European Spallation Source Study : Reference 4)

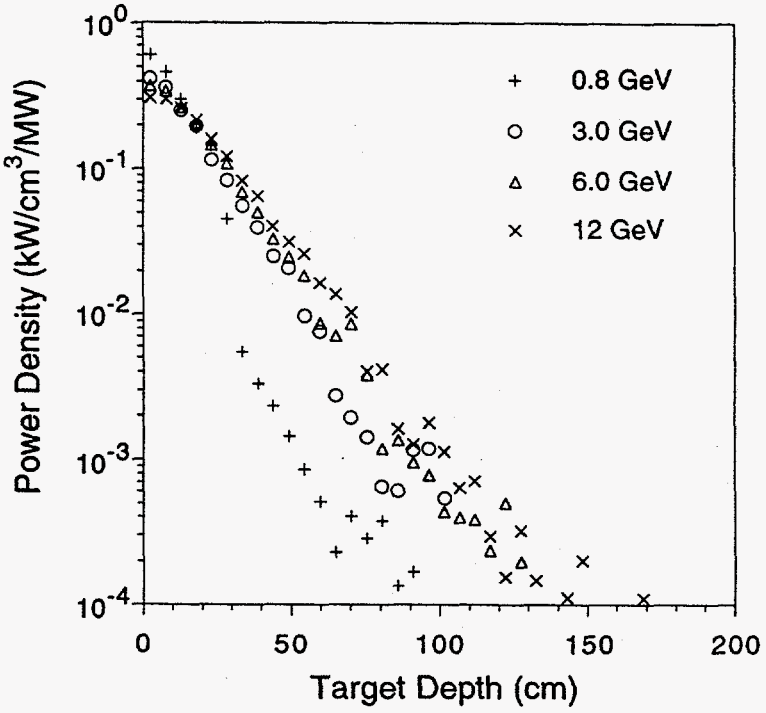

Fig. 3 Power density along the target depth for various proton energies

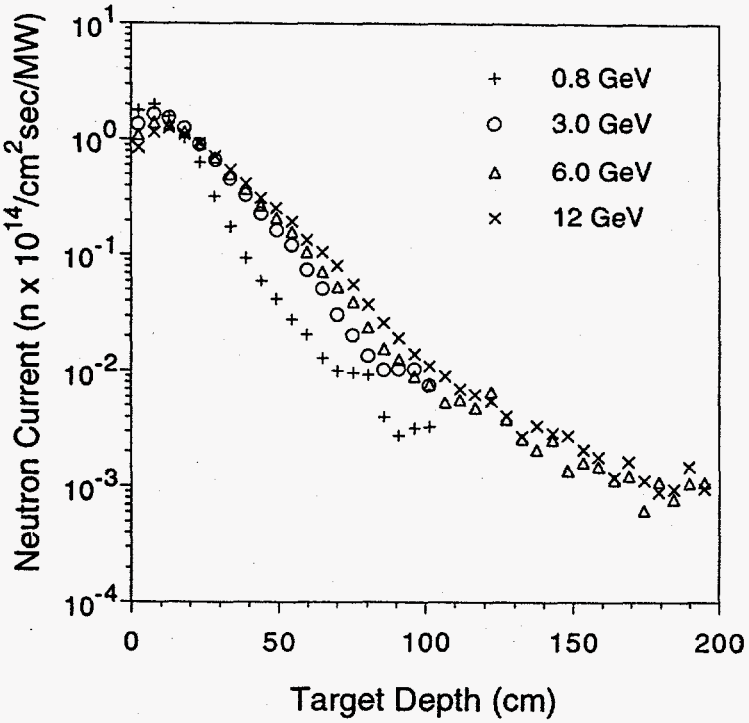

Fig. 4 Neutron current along the target for various proton energies

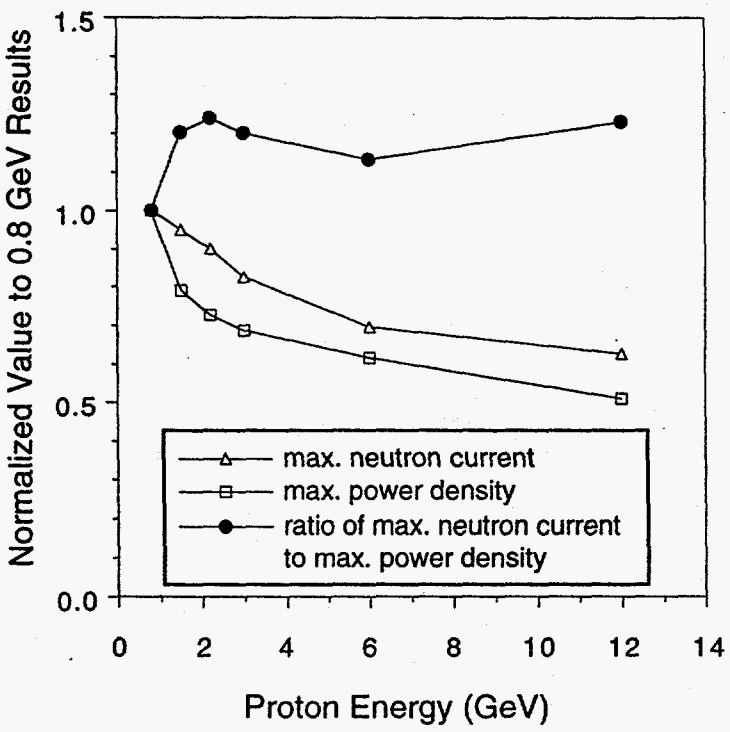

Fig. 5 Ratio of the maximum neutron current to maximum power density for various proton energies

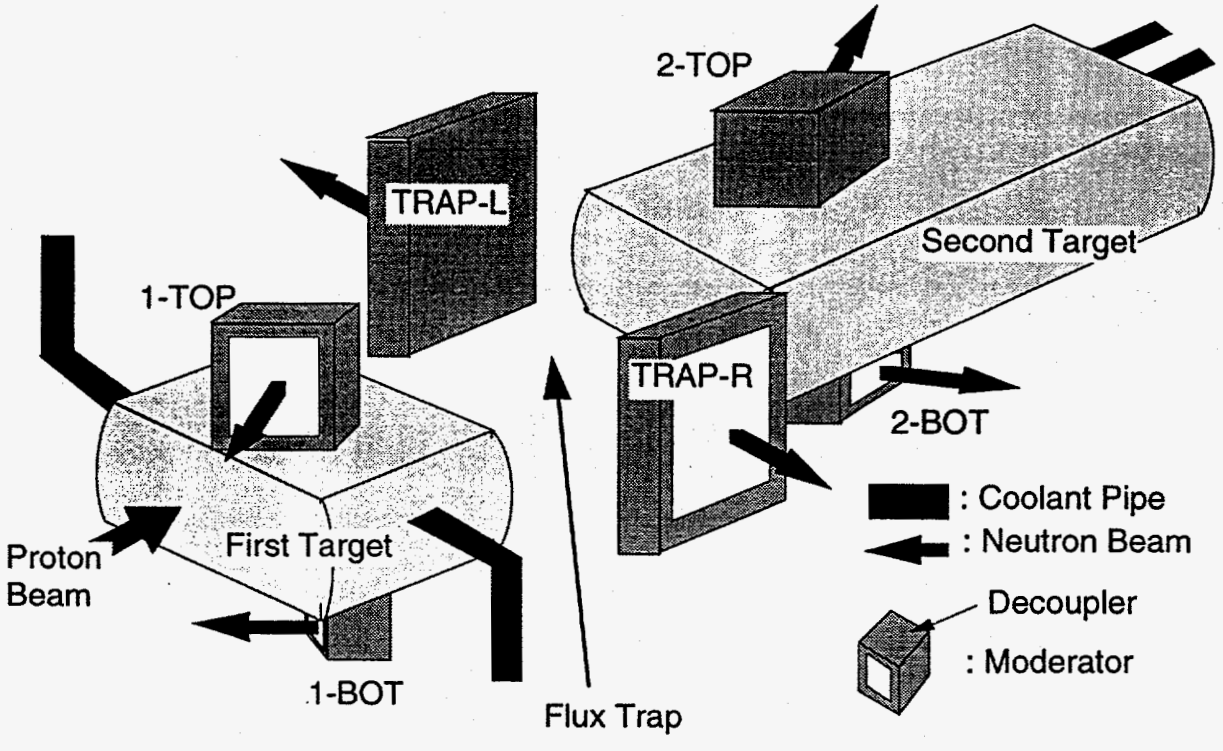

Fig. 6 Configuration of targets and moderators

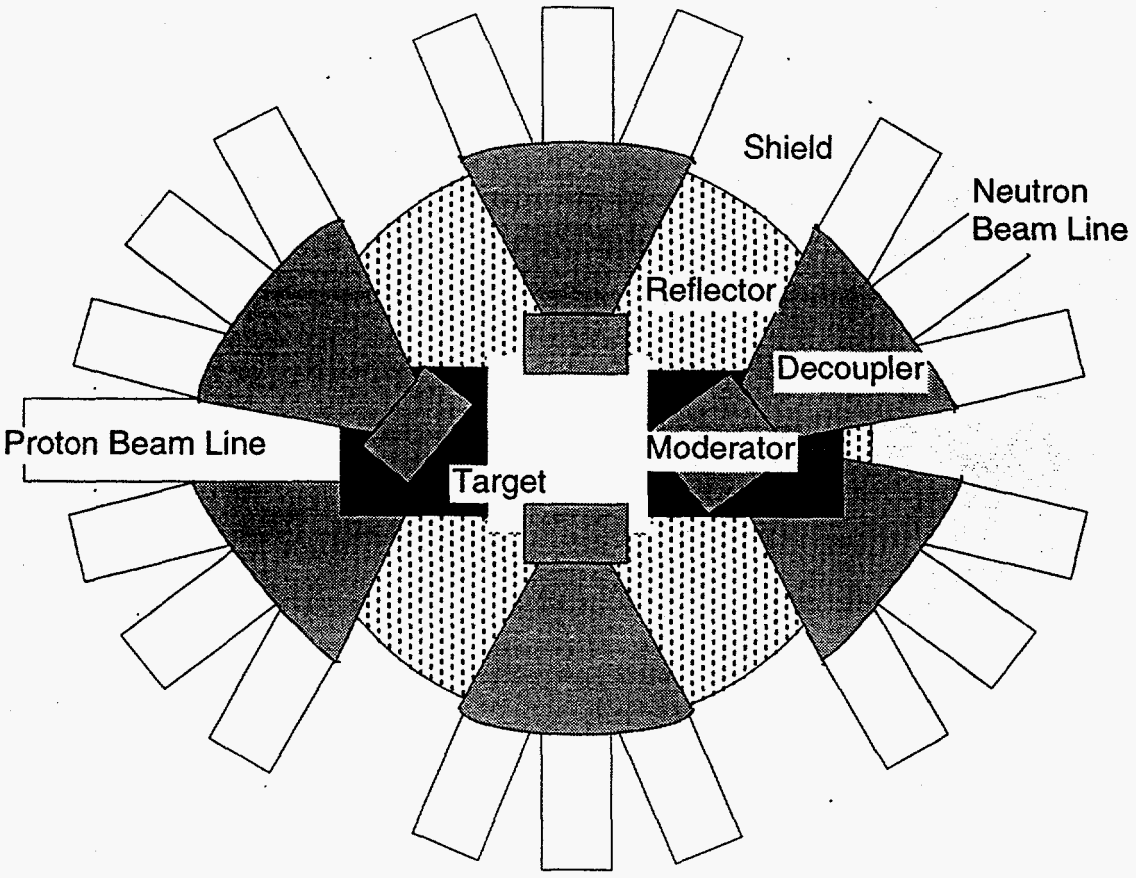

Fig. 7 Arrangement of neutron beam lines

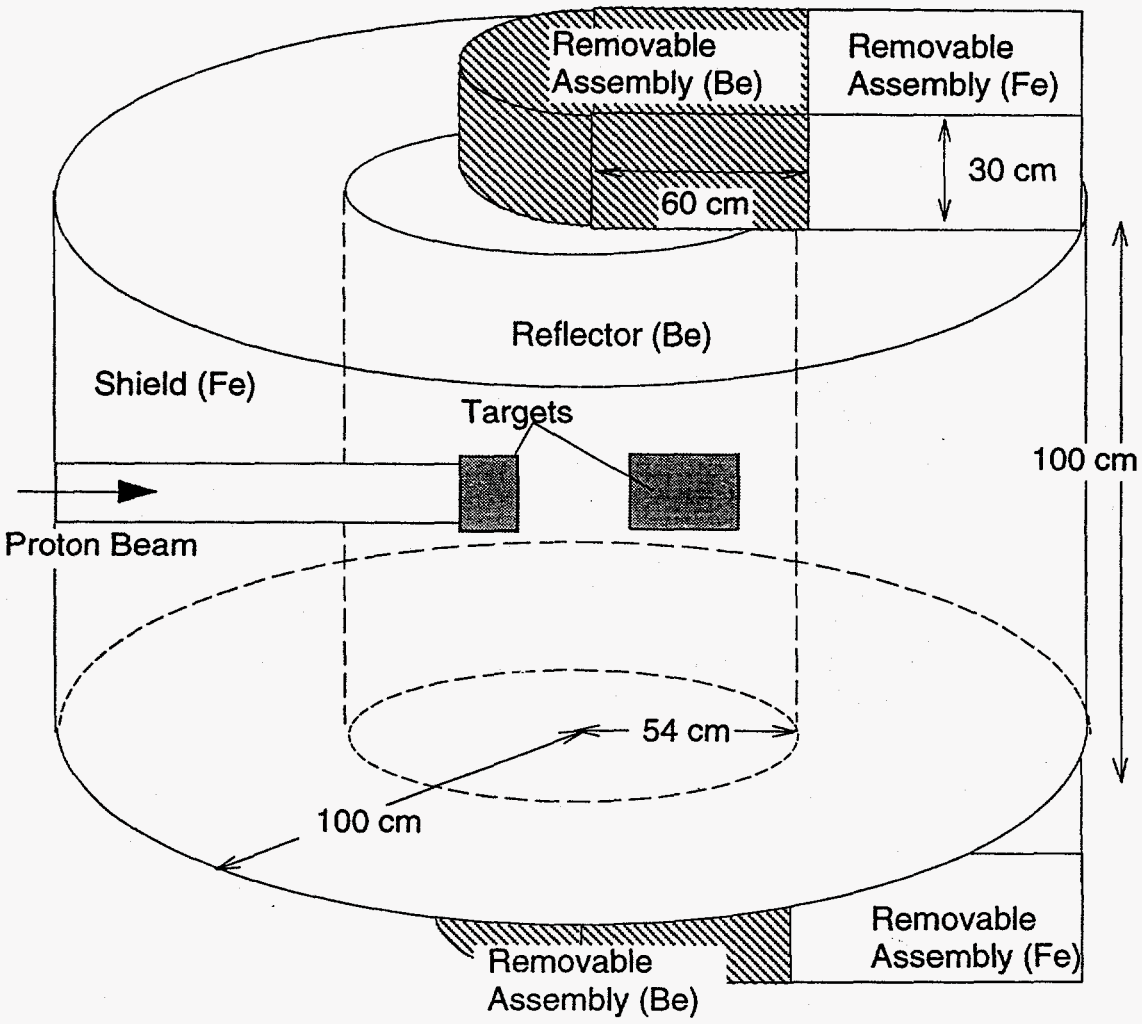

Fig. 8 Schematic of the systems surrounding the targets

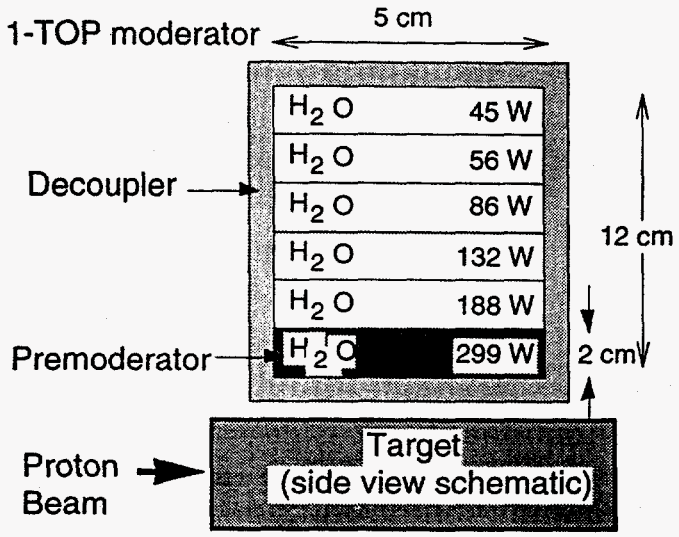

Fig. 9 (a) Power distribution of the moderator in the vertical direction

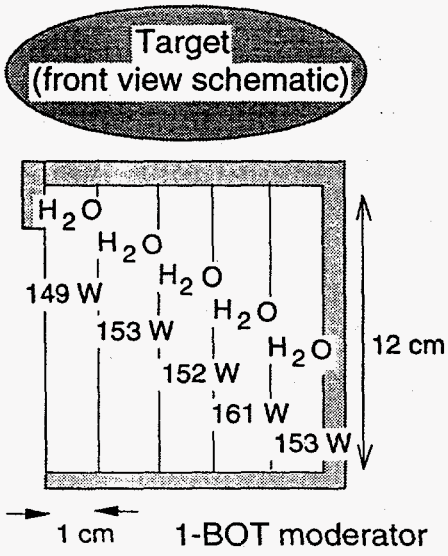

Fig. 9 (b) Power distribution of the moderator in the horizontal direction

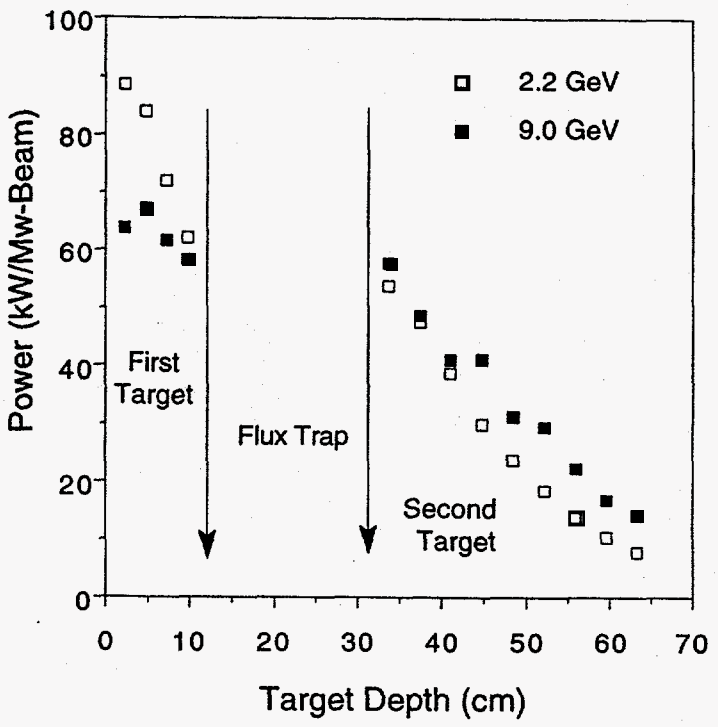

Fig. 10 Axial power distribution along the target

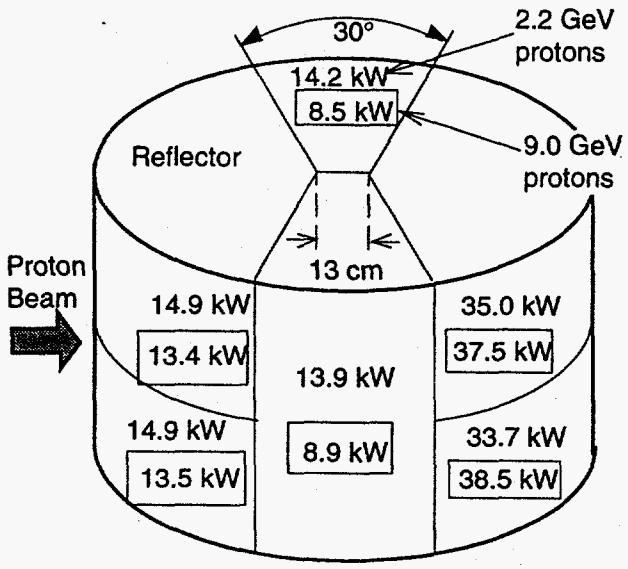

Fig. 11 Power distribution in the reflector

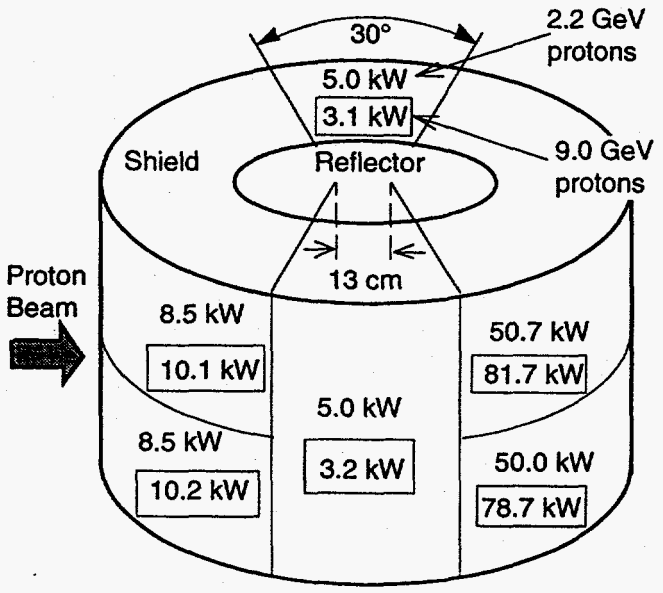

Fig. 12 Power distribution in the shield

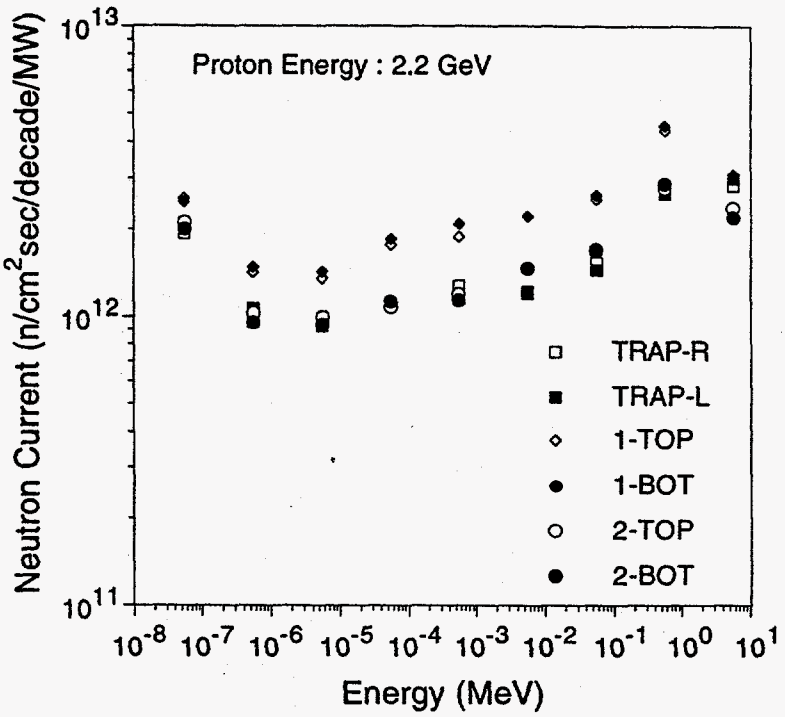

Fig. 13 Neutron beam spectra at the moderator surfaces

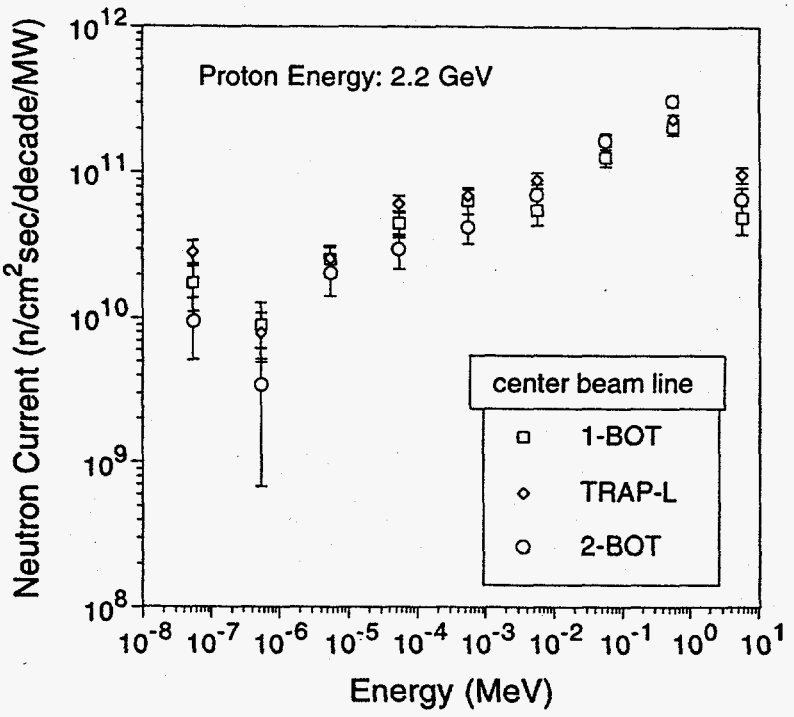

Fig. 14 Neutron beam spectra at the end of beam lines

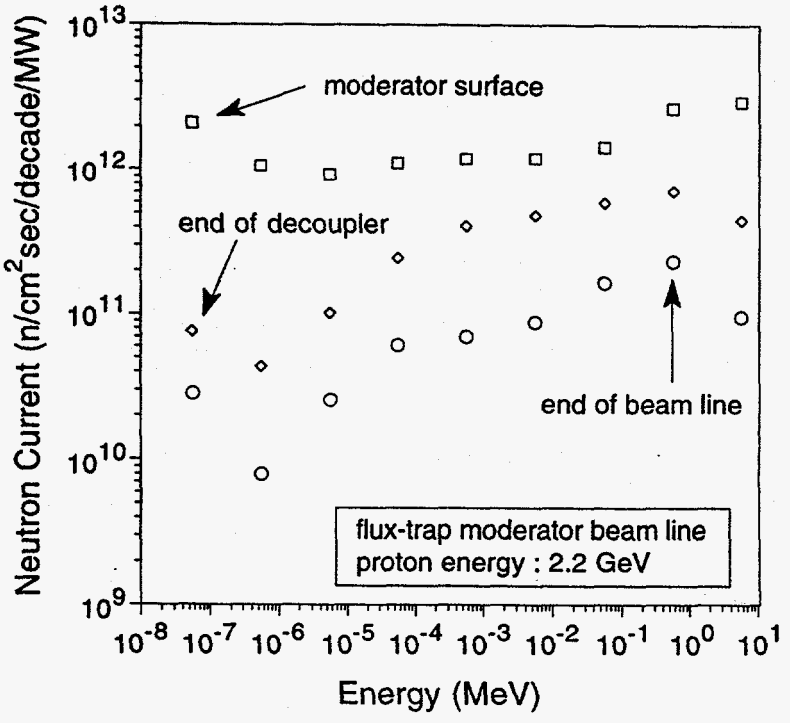

Fig. 15 Change of neutron beam spectrum along the beam line

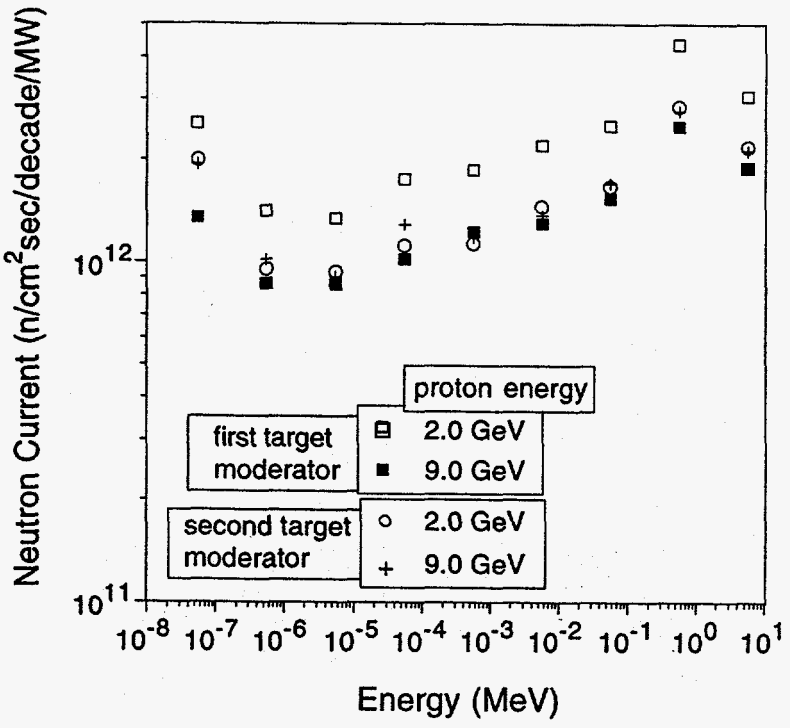

Fig. 16 Effect of proton energy on neutron beam spectra